Excitation-transfer collisions in cesium vapor: $Cs(5D_{5/2})+Cs(6S_{1/2}) \rightarrow Cs(5D_{3/2})+Cs(6S_{1/2})$

B. Keramati, M. Masters, and J. Huennekens

Department of Physics, Lehigh University, Bethlehem, Pennsylvania 18015

(Received 25 March 1988)

We report an experimental investigation of the excitation-transfer collision $Cs(5D_{5/2})+Cs(6S) \rightarrow CS(5D_{3/2})+Cs(6S)$. The upper $5D_{5/2}$ state was excited by a cw dye laser tuned to the one-photon, quadrupole-allowed $6S \rightarrow 5D_{5/2}$ transition. Since the direct $5D \rightarrow 6P$ fluorescence could not be detected with our apparatus, we monitored instead the cascade $6P \rightarrow 6S$ fluorescence. The ratio of $6P_{1/2}$ to $6P_{3/2}$ fluorescence contains information on the collisional mixing that takes place in the $5D$ levels but also includes a significant contribution from mixing in the $6P$ levels. This latter contribution could effectively be subtracted out using the results of a second experiment in which a tunable cw diode laser was used to pump the $6P_{3/2}$ state, and the same fluorescence ratio monitored. The $5D$ mixing cross section we obtain, 70 Å², is significantly larger than previous indirect determinations.

I. INTRODUCTION

Over the years there has been extensive investigation of transfer of population among alkali atom fine-structure levels in collisions with ground-state alkalis,[1-10] noble-gas atoms,[2,6-7,9-16] and diatomic molecules.[6-7,9-10,14] A complete review of theoretical and experimental work in this area up until 1975 can be found in Ref. 17. These fine-structure-level-changing collisions are important since they are among the simplest atomic-energy-transfer processes and thus represent a fundamental test for theories of atomic interactions. Recently it has also been shown that data on collisions involving transfer among fine-structure levels can provide direct information on interatomic potential curves.[18-20]

From an experimental point of view alkalis have been studied because excited states are easily accessed using tunable dye lasers. Fine-structure-level-changing collisions in various P states have been studied using direct one-photon excitation from the ground state,[3,4,11,13-16] while many D levels have also been investigated by applying two-photon or two-step excitation techniques.[1,2,5-9,12] Such studies, particularly in cesium, have allowed testing of theoretical arguments concerning the scaling of cross sections with effective principal quantum number n^*.

In the present work we report an experimental determination of the thermally averaged rate coefficient for the excitation transfer process

$$Cs(5D_{5/2})+Cs(6S_{1/2}) \rightarrow Cs(5D_{3/2})+Cs(6S_{1/2}) . \quad (1)$$
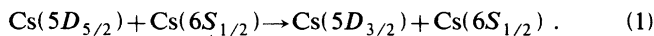
This process has not been directly studied until now because of the long wavelengths involved in both the excitation and detection stages (see Fig. 1). We sidestepped these difficulties by exciting the $5D$ levels via one-photon electric quadrupole transitions and detecting $6P \rightarrow 6S$ cascade fluorescence. Details of these techniques and the derivation of the rate coefficient from the fluorescence signals are presented in Secs. II–IV. Since $5D$ is the lowest-lying D state in cesium, measurement of this fine-structure-level-changing cross section completes this se-

quence at the low end, and therefore provides the most severe test for the n^* scaling laws. For higher D states in rubidium and cesium it was found that the fine-structure-level-changing cross section roughly scales with the geometric cross section, which was derived from a Rydberg model. For cesium $5D$, $n^*=2.55$, so core effects will presumably be significant.

Additionally, there has been some controversy over the cesium $5D$ fine-structure-level-changing cross section due to disagreement between two very indirect determinations.[21,22] The work of Wu and Huennekens yielded an anomalously low apparent upper limit on the $5D$ level mixing rate coefficient of 10^{-11} cm^{3}s^{-1} as a by-product of an experiment studying predissociation of cesium molecules.[21] At about the same time Davanloo et al.[22] obtained an apparently conflicting $5D$ mixing rate coefficient of 6.2×10^{-11} cm^{3}s^{-1} with error bars of 60%.
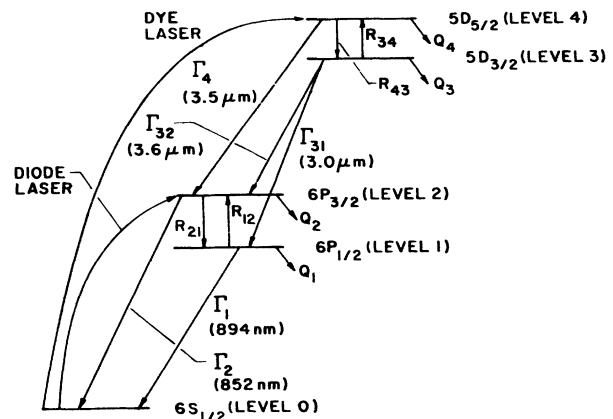

FIG. 1. Partial energy-level diagram of cesium (relative energies not to scale) showing the collisional and radiative processes considered in this work. In the figure the R's represent fine-structure mixing rates, the Q's are collisional quenching rates, and the Γ's are radiative rates. Radiative transitions are also labeled by the corresponding wavelengths.

This result was also a by-product of a photodissociation study of cesium dimers and must also be considered an indirect measurement. The mixing rate coefficient we report here, 2.6×10^{-10} cm^3 s^{-1}, is actually larger than the Davanloo et al. result. In addition, we see no evidence for the very high $5D$ quenching rate coefficient $(1.7 \times 10^{-10}$ cm^3 s$^{-1})$ which they also required to fit their data. We still do not fully understand these apparent discrepancies which will be discussed further in Sec. V.

II. EXPERIMENT

Figure 2 shows a schematic diagram of the experimental setup. Pure cesium (no buffer gas) was contained in a 2.54-cm-diameter cylindrical cell made of aluminosilicate glass. The cell was heated to 125–225 °C in a glass oven using nichrome heaters. The cell temperature was monitored by a thermocouple.

Due to the low energy of the cesium $5D$ states, they could not be pumped with the available lasers using either two-photon or two-step excitation. Instead, a tunable cw dye laser, using LDS 722 dye and pumped by 3–5 W all-lines from an argon-ion laser, was used to selectively excite the $5D_J$ levels directly from the ground state via one-photon, dipole-forbidden but electric quadrupole-allowed transitions (see Fig. 1).

Since the $5D$ levels radiate at wavelengths greater than 3 μm, which are beyond the limits of our detectors and the transmission cutoff of our glass cells, we chose to monitor the $5D$ level mixing by observing the cascade $(6P_{1/2} \rightarrow 6S)$-to-$(6P_{3/2} \rightarrow 6S)$ fluorescence ratio. However, since this ratio contains a contribution from mixing in the $6P$ levels, we were required to carry out a second experiment in which we directly excited the $6P_{3/2}$ state. This was done using a diode laser operating near 852 nm and tunable over a few nanometers by varying the diode current and temperature. Due to radiation-trapping effects described in Sec. IV, it was important that the

geometry be identical when using the two different lasers. Thus a translating mirror and a set of apertures were used to ensure that the beam paths of the two lasers through the cell were identical. The stripe of fluorescence along the laser-beam axis through the cell was imaged onto the slits of a monochromator. Again due to radiation trapping, the detection geometry plays a role in the $6P_J$ level fluorescence ratios and this point will be discussed in Sec. IV. Light through the monochromator was detected with either an S-1 or an S-20 photomultiplier. The signal was then processed through either a lock-in amplifier or an electrometer and displayed on a chart recorder. When using the diode laser, the contribution from laser scatter to the $6P_{3/2} \rightarrow 6S$ signal was determined by cooling the cell and tuning the laser off resonance. Typically this correction was a few percent.

A quartz-iodine lamp with known spectral output was used to determine the relative detection efficiency at 852.1 and 894.3 nm using the calibration procedure outlined in Ref. 23. The lamp was also used to determine the cesium-atom density using the absorption-equivalent-width technique. Since the $6P_{3/2}$ fluorescence can be partially polarized, a 45° polarizer (Polaroid HR infrared sheet polarizer) was used in front of the monochromator in conjunction with a second polarizer oriented either vertically or horizontally. This allowed measurement of the two polarization components individually in a manner that was equally sensitive to both.

III. RATE EQUATIONS AND DATA ANALYSIS

The data analysis is based upon a rate-equation approach which includes the relevant collisional and radiative rates shown in Fig. 1. We consider a five-state model including $6S_{1/2}$, $6P_{1/2}$, $6P_{3/2}$, $5D_{3/2}$, and $5D_{5/2}$, which for notational simplicity are labeled states 0, 1, 2, 3, and 4, respectively. For pumping of the $5D_{5/2}$ state we obtain the steady-state rate equations

$$\dot{n}_3 = 0 = -(\Gamma_3 + R_{34} + Q_3)n_3 + R_{43}n_4 , \tag{2}$$

$$\dot{n}_2 = 0 = -(\Gamma_2 + R_{21} + Q_2)n_2 + R_{12}n_1 + \Gamma_{32}n_3 + \Gamma_4 n_4 , \tag{3}$$

$$\dot{n}_1 = 0 = -(\Gamma_1 + R_{12} + Q_1)n_1 + R_{21}n_2 + \Gamma_{31}n_3 . \tag{4}$$

Here the n's are the number densities in the different levels, the R's are fine-structure mixing rates, the Q's are quenching rates, and $\Gamma_{31} + \Gamma_{32} \equiv \Gamma_3$ is the total radiative rate out of state 3. Due to radiation trapping, Γ_1 and Γ_2 are effective radiative rates which are much smaller than the $6P \rightarrow 6S$ natural radiative rate Γ_N. Note, however, that according to the Holstein theory of radiation trapping, Γ_1 and Γ_2 are independent of density in our range of temperatures.[24,25] The $5D \rightarrow 6P$ fluorescence is not trapped since the $6P$ states are only weakly populated by the cw pumping of the forbidden transition. This point is discussed further in Sec. IV. Since we have three equations in four unknown populations, we can solve for all population ratios and thus for the $(6P_{1/2} \rightarrow 6S)$-to-$(6P_{3/2} \rightarrow 6S)$ fluorescence intensity ratio (which we label I_1/I_2),
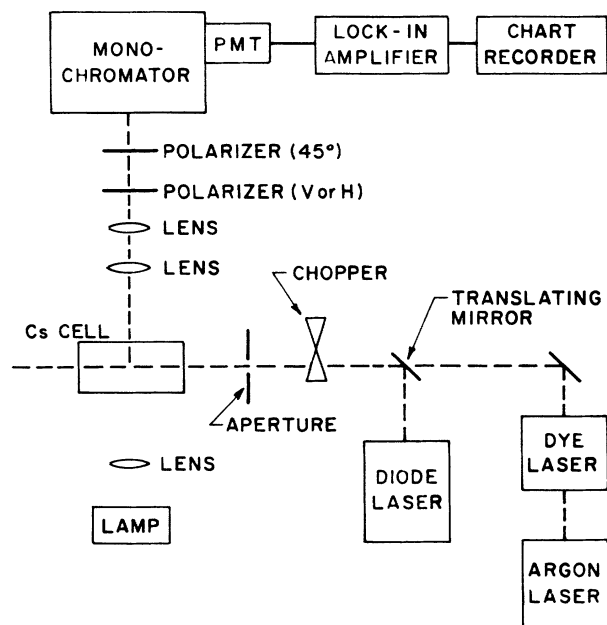

FIG. 2. Experimental apparatus.

$$\left[\frac{I_1}{I_2}\right]_{5D_{5/2}} = \frac{\epsilon_1\lambda_2\Gamma_1 n_1}{\epsilon_2\lambda_1\Gamma_2 n_2} = \frac{\epsilon_1\lambda_2\Gamma_1}{\epsilon_2\lambda_1\Gamma_2} \frac{\Gamma_{31}R_{43}(\Gamma_2+R_{21}+Q_2)+R_{21}[\Gamma_4(\Gamma_3+R_{34}+Q_3)+\Gamma_{32}R_{43}]}{(\Gamma_1+R_{12}+Q_1)[\Gamma_4(\Gamma_3+R_{34}+Q_3)+\Gamma_{32}R_{43}]+\Gamma_{31}R_{43}R_{12}} .$$ (5)

Here λ_1 and λ_2 are the transition wavelengths needed to convert from photons/sec to energy/sec, and ϵ_1/ϵ_2 is the measured relative detection system efficiency at the two wavelengths. The subscript $5D_{5/2}$ on I_1/I_2 reminds us of the particular pumping scheme.

We will argue in Sec. IV that the quenching rates can be ignored compared to the fine-structure mixing rates, so that after some algebra we can write

$$\left[\frac{I_1}{I_2}\right]_{5D_{5/2}}^{\text{no quenching}} = \frac{\epsilon_1\lambda_2}{\epsilon_2\lambda_1} \frac{(\Gamma_4\alpha_2+\Gamma_3)(R_{43}/\Gamma_4)(R_{21}/\Gamma_2)+\Gamma_{31}(R_{43}/\Gamma_4)+\Gamma_3(R_{21}/\Gamma_2)}{(\Gamma_3+(\Gamma_4\alpha_2+\Gamma_{32})(R_{43}/\Gamma_4)+(\Gamma_2/\Gamma_1)(R_{21}/\Gamma_2)\{\Gamma_3\alpha_1[1+(R_{43}/\Gamma_4)]+\Gamma_4\alpha_1\alpha_2(R_{43}/\Gamma_4)\})} .$$ (6)

Here

$$\alpha_1 \equiv R_{12}/R_{21} = (g_2/g_1)e^{-(E_2-E_1)/kT}$$

and

$$\alpha_2 \equiv R_{34}/R_{43} = (g_4/g_3)e^{-(E_4-E_3)/kT}$$

from the principle of detailed balance.

The situation in the diode-laser case is complicated by the fundamental difference between Rayleigh scatter and true fluorescence when the laser is tuned slightly off resonance. In fact, the diode laser is always off resonance because its low power (~ 8 mW) is not sufficient to burn through the vapor at line center. The complication arises because the Rayleigh scatter occurs at the laser frequency, where it is not as severely trapped as the collisionally redistributed fluorescence. Thus the Rayleigh component is characterized by one radiative rate, Γ_R, while the fluorescence is characterized by Γ_2. In general $\Gamma_2 < \Gamma_R < \Gamma_N$. However, the $6P_{3/2} \rightarrow 6S$ signal with diode-laser pumping is always the sum of the Rayleigh and

fluorescence components since they cannot be resolved by our monochromator. To properly account for the different effective radiative rates, we introduce rate equations based on Fig. 3,

$$\dot{n}_2 = 0 = \Gamma_c n_R + R_{12}n_1 - (\Gamma_2+R_{21}+Q_2)n_2 ,$$ (7)

$$\dot{n}_1 = 0 = R_{21}(n_R+n_2) - (\Gamma_1+R_{12}+Q_1)n_1 .$$ (8)

Here the laser is assumed to populate a virtual level R, which can radiate at a rate Γ_R (Rayleigh scatter) or collisionally transfer population to state 1 or state 2. The collisional rate to state 1 is R_{21} (the state $2 \rightarrow$ state 1 mixing rate), while the rate to state 2 is Γ_c, the collisional redistribution or line-broadening rate. This virtual-level model ignores coherences created between states 0 and 2 by the laser, but a correct dressed-level treatment (see Ref. 26) yields the same results as this intuitive model and demonstrates that the collisional-rate assignments used here are correct.

It can be shown from Eqs. (7) and (8) that the measured quantity $I_1/(I_2+I_R)$ is given by

$$\left[\frac{I_1}{I_2+I_R}\right]_{6P_{3/2}} = \frac{\epsilon_1\lambda_2}{\epsilon_2\lambda_1} \frac{\Gamma_1 R_{21}(\Gamma_c+\Gamma_2+R_{21}+Q_2)}{\Gamma_2[\Gamma_c(\Gamma_1+R_{12}+Q_1)+R_{12}R_{21}]+\Gamma_R[R_{12}(\Gamma_2+Q_2)+(\Gamma_1+Q_1)(\Gamma_2+R_{21}+Q_2)]} .$$ (9)

Since $\Gamma_c \gg R_{21}$ always (collisional dephasing cross sections are always much larger than those of any other collisional process), we can derive the following equation valid in the limit of no quenching:

$$\left[\frac{I_1}{I_2+I_R}\right]_{6P_{3/2}}^{\text{no quenching}} = \frac{\epsilon_1\lambda_2}{\epsilon_2\lambda_1} \frac{(R_{21}/\Gamma_2)(1+\Gamma_2/\Gamma_c)}{1+\alpha_1(\Gamma_2/\Gamma_1)(R_{21}/\Gamma_2)+(\Gamma_R/\Gamma_c)\{1+(R_{21}/\Gamma_2)[1+\alpha_1(\Gamma_2/\Gamma_1)]\}} .$$ (10)

Equations (6) and (10) are the basic expressions used to analyze our data. However, it is instructive to look at the low-density limits of these expressions where collisional rates can be neglected compared to radiative rates (i.e., $\Gamma_1 \gg R_{12}$, $\Gamma_2 \gg R_{21}$, $\Gamma_3 \gg R_{34}$, $\Gamma_4 \gg R_{43}$),

$$\left[\frac{I_1}{I_2}\right]_{5D_{5/2}}^{\text{low density}} = \frac{\epsilon_1\lambda_2}{\epsilon_2\lambda_1}\left[\frac{R_{21}}{\Gamma_2}+\frac{\Gamma_{31}}{\Gamma_3}\frac{R_{43}}{\Gamma_4}\right] ,$$ (11)

$$\left[\frac{I_1}{I_2+I_R}\right]_{6P_{3/2}}^{\text{low density}} = \frac{\epsilon_1\lambda_2}{\epsilon_2\lambda_1}\frac{R_{21}}{\Gamma_2}\left[\frac{1+(\Gamma_2/\Gamma_c)}{1+(\Gamma_R/\Gamma_c)}\right] ,$$ (12)

These expressions are linear in cesium density over the

range of temperatures where Γ_2 is independent of density, and amount to neglect of the back-transfer terms. The first term within the square brackets in Eq. (11) represents the mixing which occurs in the $6P$ levels, while the second term represents the $5D$ level mixing (Γ_{31}/Γ_3 is simply a radiative branching factor). The term in large parentheses on the right-hand side of Eq. (12) represents the effects of the Rayleigh scattering. It can be seen that this term becomes equal to unity when $\Gamma_R = \Gamma_2$, which occurs in the optically thin case where $\Gamma_2 = \Gamma_R = \Gamma_N$, but also when trapping of the Rayleigh scatter is comparable to that of the fluorescence (i.e., for excitation on resonance). When it is justified to replace this bracket by unity, a particularly simple result can be obtained for the
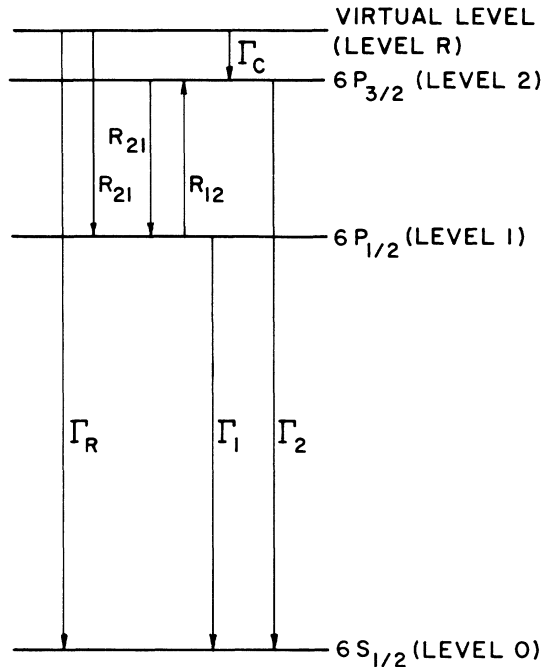
FIG. 3. Simplified model used for constructing the rate equations (7) and (8). The level "R" is a virtual level populated by the laser. See text for a complete description.

$5D_{5/2} \rightarrow 5D_{3/2}$ mixing rate,

$$R_{43} = k_{43}[\text{Cs}]$$

$$= \frac{\Gamma_4 \Gamma_3}{\Gamma_{31}} \frac{\epsilon_2 \lambda_1}{\epsilon_1 \lambda_2} \left[\left[\frac{I_1}{I_2} \right]_{5D_{5/2}} - \left[\frac{I_1}{I_2 + I_R} \right]_{6P_{3/2}} \right], \quad (13)$$

where [Cs] is the cesium atom density and k_{43} is the mixing rate coefficient. In this form it is easy to see that taking measurements using the two different pumping schemes allows a straightforward subtraction of the effects of $6P$ state mixing.

Figure 4 shows a plot of our measured values of

$$\left[\frac{I_1}{I_2} \right]_{5D_{5/2}}$$

and

$$\left[\frac{I_1}{I_2 + I_R} \right]_{6P_{3/2}}$$

versus cesium density. As can be seen, most of our data is within the linear regime. Nevertheless, the back-transfer terms cannot be ignored without introducing errors of the order of 30%, so that Eqs. (6) and (10) were used for the analysis. The procedure was to carry out a least-squares fit of Eq. (10) to our measured values of $[I_1/(I_2+I_R)]_{6P_{3/2}}$ versus cesium density. This yielded a best value for $k_{21}/\Gamma_2 \equiv R_{21}/(\Gamma_2[\text{Cs}])$. This value was in turn used in a least-squares fit of Eq. (6) to our measurements of $(I_1/I_2)_{5D_{5/2}}$ versus density.

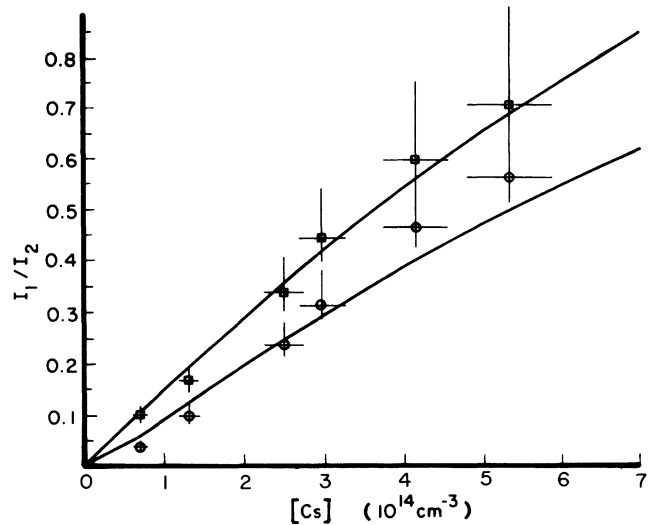The only difficulty which remained to be overcome in

FIG. 4. Plot of $(I_1/I_2)_{5D_{5/2}}$ and $[I_1/(I_2+I_R)]_{6P_{3/2}}$, represented by squares and circles, respectively, vs cesium density. The solid curves are least-squares best fits of Eqs. (6) and (10) to the data. Error bars have been given for each point.

order to carry through this procedure was to obtain values for Γ_R/Γ_c and Γ_2/Γ_1 to use in Eq. (10). Now $\Gamma_R < \Gamma_N = 3.26 \times 10^7$ sec^{-1} (from Ref. 27) and $\Gamma_c = 7.51 \times 10^{-7}[\text{Cs}]$ (from Ref. 28). Therefore, over the density range of our experiment, 7×10^{13} to 6×10^{14} cm^{-3}, the Γ_R/Γ_c term contributes between 7% and 62% to the denominator of Eq. (10). In fact, Γ_R can be estimated reasonably accurately since the diode-laser frequency was set to maximize the sensitized fluorescence signal at 894.3 nm. This maximum occurs approximately when the laser power absorbed in the observation region is maximized. This point is found by maximizing the function $I_0(e^{-k_v L} - e^{-k_v(L+\Delta L)})$ with respect to k_v, which is the absorption coefficient at frequency v. I_0 is the incident intensity, and the observation zone extends from L to $L + \Delta L$ with respect to the entrance window. The laser detuning which peaks the fluorescence will be such that

$$k_v = (\Delta L)^{-1} \log_e[(L + \Delta L)/L] .$$

For our typical values of L and ΔL we find $k_v \sim 0.31$ cm^{-1}. The escape probability at this frequency is $e^{-k_v R}$ where R is the cell radius. Thus $\Gamma_R \sim \Gamma_N e^{-k_v R} \sim 2.36 \times 10^7$ s^{-1} at all densities. Γ_2/Γ_1 can be calculated accurately from the Holstein theory of radiation trapping[24,25], which has been verified for similar situations in sodium.[29,30] Thus we obtain $\Gamma_2/\Gamma_1 = 0.993$, independent of density. Note that because the trapped radiative rates depend critically on the excitation and detection geometry as well as on the atom density, it is crucial that both the diode- and dye-laser experiments be carried out with identical geometries (see also Sec. IV). Under these conditions, Γ_2 and Γ_1 will be independent of the state that is pumped. Note also that Γ_2/Γ_c can always be neglected in Eq. (10) under our conditions.

IV. RESULTS

Finally, from the least-squares fit of the $(I_1/I_2)_{5D_{5/2}}$ data and radiative rates from Ref. 27 we obtain our best value of k_{43}, which is the thermally averaged rate coefficient at $T \sim 425$ K,

$$k_{43} = 2.6 \times 10^{-10} \text{ cm}^3 \text{ s}^{-1} \pm 40\% . \quad (14)$$

Using the mean thermal velocity

$$\bar{v} = \left[\frac{8RT}{\pi} \frac{M_1 + M_2}{M_1 M_2} \right] \sim 3.67 \times 10^4 \text{ cm s}^{-1}$$

we can calculate an average cross section defined by

$$\sigma_{43} \sim k_{43}/\bar{v} = 70 \text{ Å}^2 \pm 40\% . \quad (15)$$

Before proceeding to a discussion of these results a few additional comments concerning radiation trapping, Rayleigh scatter, and quenching are required, followed by a short discussion about the uncertainty estimates.

A. Radiation trapping and Rayleigh scatter

Radiation trapping in alkali vapors has been studied extensively in recent years.[29,30] These studies have shown that the Holstein theory[24,25] gives accurate analytic expressions for effective radiative decay rates under certain well-defined circumstances. However, trapping is very sensitive to geometry and care must be exercised when applying the Holstein theory to actual experiments. Not only is the cell geometry important, but so too is the excitation and detection geometry.

In our experiment the cesium densities were sufficiently high that the Holstein pressure-broadening limit was always appropriate, and the theory yields $6P \rightarrow 6S$ radiative decay rates $\Gamma_{\text{eff}} \sim 8 \times 10^4 \text{ sec}^{-1}$ independent of density.[29] This decay rate corresponds to a "fundamental-mode" excitation scheme which is realized with an unfocused laser beam roughly filling the cell cross section. Use of focused laser beams as in this experiment results in longer decay times or slightly smaller decay rates. Nonetheless, Γ_{eff} should be approximately constant with density so that k_{21}/Γ_2 should be constant. The approximate linearity of the $[I_1/(I_2 + I_R)]_{6P_{3/2}}$ data in Fig. 4 demonstrates that this is reasonable. We have found two previous measurements of the $6P_{3/2} + 6S \rightarrow 6P_{1/2} + 6S$ cross section.[31,32] Bunke and Seiwert[31] obtained $\sigma_{21} = 13$ Å^2, while Czajkowski and Krause[32] obtained $\sigma_{21} = 31$ Å^2. Using these two values in our expression for $k_{21}/\Gamma_2 = 1.40 \times 10^{-15}$ cm^3 obtained from the fit of the $[I_1/(I_2 + I_R)]_{6P_{3/2}}$ data in Fig. 4, we obtain $\Gamma_2 \sim 3.4 \times 10^4$ and 8.1×10^4 s^{-1}, respectively. Thus we can conclude that the trapping problem is being handled in a reasonable fashion. However, our calculation of Γ_2 under these conditions is not sufficiently precise to establish a preference for one or the other previous values of σ_{21}.

The measured intensity ratios are also sensitive to detection geometry. Photons take longer to diffuse to locations further from the laser axis, and therefore the probability that a fine-structure-level-changing collision

has occurred is also greater further out. Thus I_1/I_2 increases with offset of the detection region from the laser axis. However, as long as the $5D \rightarrow 6P$ fluorescence remains untrapped, and the diode- and dye-laser beams follow the same path, the value of k_{43} obtained from our measurements should be independent of detection position.

During the course of our measurements we realized that detection of light from a strip-shaped region perpendicular to the laser beams would result in intensity ratios that were far less sensitive to small offsets between the two beams. Only our data taken using this detection scheme are plotted in Fig. 4. Earlier data taken when we imaged a strip oriented along the laser beams must be fit using a smaller value of k_{21}/Γ_2 (since Γ_2 was larger). Nevertheless, the less accurate value of k_{43} obtained from these earlier data is consistent with our reported value from the later measurements to within combined error bars.

Although the $5D \rightarrow 6P$ fluorescence is produced by pumping a forbidden transition with a weak cw laser, it is important to verify that the slight radiation trapping on these transitions is not affecting our results. To do this we must first calculate the $6P_J$ level populations corresponding to the case of dye-laser pumping. The $6P$ populations can be obtained in the diode-laser case from the known laser power absorbed; i.e.,

$$n_{6P} = (P/h\nu)/(\Gamma_{\text{eff}} V_{\text{eff}}) .$$

Here $P = P_0(1 - e^{-k_\nu L})$ is the laser power absorbed in the cell of length L, and V_{eff} is the "trapping volume." We have already shown that $k_\nu \sim 0.31$ cm^{-1} for diode-laser pumping and $\Gamma_{\text{eff}} \sim 8 \times 10^4$ s^{-1} for all cesium densities studied. We use $V_{\text{eff}} \sim \pi r_{\text{eff}}^2 L$ with $r_{\text{eff}} = 0.3$ cm. This value, which represents the spatial extent of the $6P$ atoms, is intentionally small in order to calculate a maximum $5D \rightarrow 6P$ trapping effect. In this way we obtain $6P$ atom densities of $\sim 2.6 \times 10^{11}$ cm^{-3} with diode-laser pumping. The $6P_J$ level populations with dye-laser pumping are obtained by comparing the $6P_J$ level fluorescence with that obtained using the diode laser. In this manner, we obtain a maximum $6P_{3/2}$ density of 2.7×10^{10} cm^{-3} using the dye laser. We then used these calculated $6P_J$ densities to determine trapping factors from the Milne theory,[33] which has been shown to provide accurate values in the low-optical-depth case.[34] The $6P$ density is maximum for the highest cesium density where our calculation yielded a trapping correction of 22%. Note that this is a worst case (other data points are affected by substantially smaller amounts), and that the calculation was carried out using approximations that deliberately overestimated the effect.

Although the calculation above provides an upper limit to the effects of $5D \rightarrow 6P$ fluorescence trapping, we were able to show experimentally that such effects could be neglected under our conditions. We measured I_1/I_2 as a function of laser power for both diode- and dye-laser pumping. Each component is linear in laser intensity and therefore the ratios are obviously independent of intensity. Since $5D \rightarrow 6P$ trapping decreases with decreasing in-

tensity, it is clear that any effect this trapping might have on our results is small, in agreement with the preceding calculation. For these reasons, no attempt was made to correct our results for $5D \rightarrow 6P$ trapping.

We indicated in Sec. III how the radiative rate appropriate to Rayleigh scatter could be estimated, and how this value was approximately independent of density because the diode laser frequency was always set to maximize the sensitized fluorescence. In general, errors in Γ_R are not critical since $\Gamma_R / \Gamma_c \lesssim 0.25$ for $[\text{Cs}] > 1.25 \times 10^{14}$ cm^{-3} where most data was taken. However, the Rayleigh scatter is also partially polarized and is therefore anisotropic. Additionally, the fluorescence is anisotropic due to trapping. The detection system was made equally sensitive to both polarizations as described in Sec. II, and the anisotropies calculated as described in Refs. 4 and 26. For Rayleigh scattering and fluorescence, the enhancement of intensity in the detection direction (relative to an isotropic distribution) is 18% and 14–27%, respectively, and therefore the two effects almost cancel. We estimate that these effects (which we did not correct for) bias our results by less than 10%.

Intensities were always recorded for both the vertical and horizontal polarizations. In all cases reported intensities represent the sum of these two components.

B. Quenching

Quenching terms have been neglected in Eqs. (6) and (10) despite fairly large quenching rates reported for higher D levels.[1,35,36] This is because the $5D$ and $6P$ levels are quite isolated (each is more than 2700 cm^{-1} away from the nearest level). Thus quenching by ground-state cesium atoms, where the excitation energy can only couple to translational motion, should be negligible in this case where $kT \lesssim 300$ cm^{-1}. The fact that the data can be well fit without quenching terms is indicative that this approximation is justified.

Quenching by Cs$_2$ molecules in processes such as

$$\text{Cs}_2(X\,{}^1\Sigma_g^+) + \text{Cs}(6P, 5D) \rightarrow \text{Cs}_2^* + \text{Cs}(6S) \qquad (16)$$
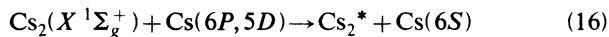
(where Cs$_2^*$ is an excited molecule) must be considered since the rate coefficients can be almost gas kinetic [$k \sim 3 \times 10^{-9}$ cm^3 s^{-1} for the analogous process in Na$_2$ (Ref. 37)]. However, for $T = 225\,°\text{C}$, which is roughly the highest temperature at which we took data, [Cs$_2$] is only 10^{13} cm^{-3} according to the Nesmeyanov relation.[38] Thus quenching by Cs$_2$ molecules could not compete with radiative decay from the $5D$ levels. Due to trapping, radiative decay from the $6P$ levels is slower, but still the quenching terms remain insignificant over our range of temperatures. Even at higher temperatures, $6P$ state quenching would affect both laser-pumping situations equally and would therefore effectively cancel.

Excited-atom–excited-atom collisions such as

$$\text{Cs}(5D_{5/2}) + \text{Cs}(6P_{1/2}) \rightarrow \text{Cs}(8P_{3/2}) + \text{Cs}(6S) , \qquad (17)$$

which is out of resonance by only 17 cm^{-1}, and collisions

involving two $6P$ atoms must also be considered here, even though we are pumping with a weak cw laser. Such collisions could change the $5D$ and $6P$ atom decay rates or change the fluorescence ratio I_1/I_2 through cascade contributions. Contributions from these effects can be calculated using the $6P_j$ level populations obtained in Sec. IV A on radiation trapping. $5D$ level populations are smaller than those of the $6P$ levels by the ratio $\Gamma_{6P\,\text{eff}}/\Gamma_{5D}$. Using an extreme value for the excited-atom–excited-atom collision cross section of 10^{-13} cm^2, we can show that the fluorescence ratio I_1/I_2 cannot change by more than 10% except for diode-laser pumping at the lowest cesium density studied. For this one point the effect could be 20%. However, these calculation assume the very large excited-atom–excited-atom cross section given above, and that all more highly excited atoms produced by such processes cascade down through the $6P$ levels. For dye-laser pumping, excited-atom populations are substantially smaller than in the diode-laser case and all such effects can be shown to be negligible.

Just as in the case of $5D \rightarrow 6P$ fluorescence trapping, a calculation is used to provide an upper limit to the effect of excited-atom–excited-atom collisions. However, laser power dependences give experimental verification that these processes can be neglected here. In particular, we observe that all signals are linear in laser power, whereas any contribution from excited-atom–excited-atom collisions would scale quadratically.

Finally, since we are using sealed cells, we must worry about quenching by impurities; especially diatomic molecules. We can immediately state that any such effects are small, since we can calculate the $6P$ state decay rates from our measured fluorescence ratios and the known values of the $6P_{3/2} + 6S \rightarrow 6P_{1/2} + 6S$ cross section.[31,32] These values are in good agreement with decay rates obtained from radiation-trapping theory. In fact, the $6P$ state decay rates calculated from our data clearly provide an upper limit to the quenching rates. Note that quenching of $6P$ levels by impurities will not affect our results in any event, as long as the quenching is the same for both excitation conditions. If we assume similar quenching cross sections for the $5D$ levels we then establish that the relatively short $5D$ state lifetime is affected by less than 10% due to quenching. In addition, we can argue against quenching by permanent gases in the cell, since such gases would also cause fine-structure-level mixing which would result in nonzero y axis intercepts in Fig. 4. Quenching by species that outgas from the cell walls when they are heated is a more difficult effect to eliminate from consideration. The densities of such gases would probably scale differently with temperature than that of cesium, and thus probably could be detected by significant nonlinearity of the data of Fig. 4. To experimentally test for effects of impurities, we had a second sealed quartz cell made commercially. We observed no systematic differences in fluorescence ratios measured in the two cells. Since it is unlikely that impurity concentrations would be the same in the two cells, it seems reasonable to conclude that impurities cause no significant quenching in either cell.

C. Determination of cesium density

The cesium-atom number density was measured directly using the absorption-equivalent-width technique on both the $6S_{1/2} \rightarrow 6P_{1/2}$ and $6S_{1/2} \rightarrow 6P_{3/2}$ transitions. Since we operated in the pressure-broadening limit, we used the self-broadening rate Γ_c calculated by Carrington et al.[28] These calculations for $J = \frac{1}{2}$ to $J = \frac{1}{2}, \frac{3}{2}$ transitions were found to be accurate to within 15% experimental uncertainties in the analogous Na case.[4] Densities obtained from equivalent widths were self-consistent and agreed with those obtained from the Nesmeyanov vapor pressure formula to within about a factor of 2. This discrepancy is not considered significant since the vapor-pressure technique is notoriously unreliable for determining alkali densities. In particular, this technique may suffer from serious errors in the vapor-pressure formula itself, or the temperature measured may not be that of the coldest point in the cell. The equivalent-width technique is a direct measurement which only depends on well-known line-broadening parameters. Thus we believe that densities determined from equivalent width measurements are more reliable than those obtained from vapor-pressure formulas and, in particular, are less likely to suffer from systematic errors.

D. Uncertainties

An estimate of the uncertainty in our measured rate coefficient can be obtained by looking at Eqs. (10) and (6). Starting with Eq. (10), we estimate that the ratio of detection efficiencies is accurate to $\sim 5\%$, while the uncertainty in Γ_2/Γ_1 from the Holstein theory is probably on the order of 10%. Since the $6P_{3/2} + 6S \rightarrow 6P_{1/2} + 6S$ excitation-transfer process is exothermic by 554 cm^{-1}, which is not small compared to $kT \sim 300$ cm^{-1}, there will not in general be a Boltzmann velocity distribution in the $6P_{1/2}$ state. Therefore

$$\alpha_1 \equiv (g_2/g_1)e^{-(E_2-E_1)/kT}$$

in the back-transfer term should be described by an effective temperature rather than the cell temperature. Since we have no reasonable method for estimating this effective temperature, which is also a function of atom density, we use the cell temperature to compute α_1 but assign it a relatively large uncertainty of a factor of 2. We consider this to be a conservative overestimate of the error since the 554 cm^{-1} heat liberated in the collision will be shared by the two colliding atoms, and additional thermalizing collisions will further reduce the effective temperature. Since the cell temperature is a lower bound on the effective temperature in α_1, the assigned uncertainty in α_1 is $(+100\%, -0\%)$. This is the cause of the asymmetry in our error bars in Fig. 4.

The Rayleigh term Γ_R/Γ_c involves both the broadening rate and our calculation of the trapping at the diode-laser frequency. Thus we estimate the uncertainty in this term at $\sim 30\%$. Finally the fluorescence ratio itself is accurate to $\sim 5\%$. We assign a random error of 10% to our determination of the cesium density (the systematic error in this quantity could be more like 20%). In this

way we assign an overall statistical error to each measured value of $[I_1/(I_2+I_R)]_{6P_{3/2}}$ in Fig. 4. These are shown as error bars in both x and y for each point in Fig. 4.

The value of k_{21}/Γ_2 obtained from our fitting routine has a statistical error of 4%. We use this uncertainty in Eq. (6) and estimate the errors in α_1, Γ_2/Γ_1, ϵ_1/ϵ_2, and the measured fluorescence ratio as before. α_2 is probably accurate to 10% since the $5D$ state fine-structure splitting is only about $0.3kT$. Γ_4 and the Γ_3's were taken from Warner,[27] and we estimate them to be accurate to $\sim 10\%$. Ratios of the Γ's are expected to be much better. We thus obtain an overall error for each $[I_1/I_2]_{5D_{5/2}}$ point. Our fitting procedure then yields an uncertainty of $\sim 40\%$ in k_{43}. We believe this is sufficiently large to also account for the systematic errors in the density determination and the relative detection efficiency, etc.

V. DISCUSSION

The cesium $5D_{5/2} \rightarrow 5D_{3/2}$ fine-structure-level-changing collision rate coefficient reported here $(2.6 \times 10^{-10}$ cm^{3}s$^{-1})$ is significantly larger than the upper limit obtained from the work of Wu and Huennekens[21] $(10^{-11}$ cm^{3}s$^{-1})$, and somewhat larger than the value 6.2×10^{-11} cm^{3}s^{-1} obtained by Davanloo et al.[22]

In the experiment of Wu and Huennekens, cesium molecules were pumped with fixed frequency lines from an argon-ion laser. Some of the excited molecules then predissociated or collisionally transferred excitation to produce excited atoms in the $5D_{5/2}$ and $5D_{3/2}$ levels. The $5D$ level populations were then detected by monitoring the quadrupole-allowed $5D \rightarrow 6S$ fluorescence. At all temperatures studied (representing cesium densities up to 10^{17} cm^{-3}), the ratio of $5D_{5/2} \rightarrow 6S$ fluorescence to $5D_{3/2} \rightarrow 6S$ fluorescence was approximately 2:1. However, the expected thermal equilibrium fluorescence ratio is 1.1:1. To verify that the discrepancy did not result from incorrect transition probabilities, the experiment was also carried out in a cell containing $\frac{1}{2}$ atm. of neon buffer gas. In this case the ratio of 1.1:1 was obtained. The implication of these results is that the collisional mixing rate $R_{43} = k_{43}[\text{Cs}]$ is less than the radiative rate $\Gamma_4 = 8.4 \times 10^5$ s^{-1} for $[\text{Cs}] < 10^{17}$ cm^{-3}. This yields the upper limit given above. In the present work we also observed the $5D$ quadrupole transitions following pumping of the cesium vapor with the argon-ion laser lines 488 and 514 nm in order to verify the previous results in our cell and under our experimental conditions. Again we saw the fluorescence ratio of 2:1 reported by Wu and Huennekens. At present, we are at a loss to reconcile the 2:1 fluorescence ratio (independent of density) with our current measurements of the $5D$ fine-structure mixing.

Davanloo et al.[22] obtained a value for the $5D$ state fine-structure mixing rate coefficient of 6.2×10^{-11} cm^{3}s^{-1}. This measurement also involved pumping of cesium molecules and observing dissociation to the $5D$ levels. in this case, however, the excitation was with a high-power, pulsed laser. The $5D_J$ level populations as a function of time were monitored by using a second (de-
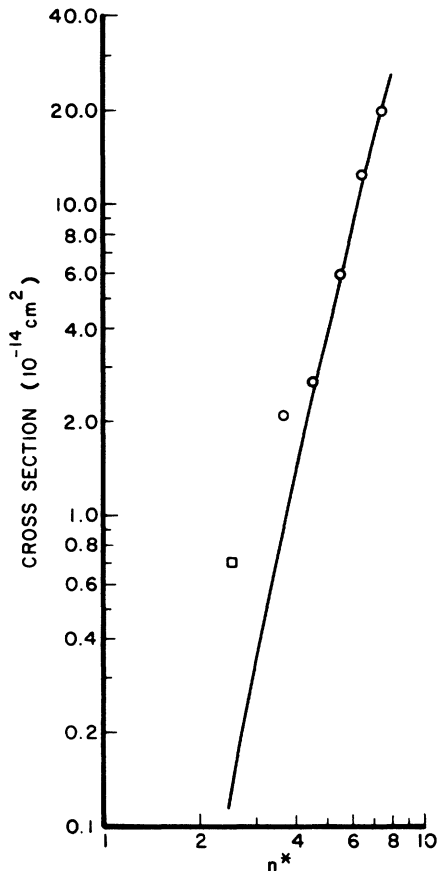
FIG. 5. Plot of cross sections for the fine-structure-level-changing collisions $Cs(nD_{5/2})+Cs(6S)\rightarrow Cs(nD_{3/2})+Cs(6S)$ vs effective principal quantum number n^*. The data for $n=6-10$ (circles) are taken from Ref. 1, while the $n=5$ case (square) is from the present work. The solid line is a plot of r^2 from Eq. (18).

cipal quantum number n^*. This figure is the same as Fig. 4 of Ref. 1, except that our result for the $5D$ levels has been added. The data for the $6D-10D$ states is that of Tam et al.[1] The geometric cross section can be approximated by the hydrogenic expectation value of the square of the orbit radius given by[39]

$$r^2=\tfrac{1}{2}n^{*2}[5n^{*2}+1-3l(l+1)]a_0^2 .$$ (18)

Tam et al. found that for $n=7-10$, $\sigma_{43}\approx r^2$, while for $n=6$ the cross section was 2.6 times larger than r^2. Equation (18) is plotted in Fig. 5 as a solid curve. For the $5D$ levels, where $n^*\approx 2.55$, we calculate $r^2=14$ Å^2. Our measured value is about 5 times larger. Thus our current measurement seems consistent with the trend shown by the $6D$ mixing rate.

VI. CONCLUSIONS

In this paper we have reported an experimental value for the $Cs(6S)+Cs(5D_{5/2})\rightarrow Cs(6S)+Cs(5D_{3/2})$ fine-structure-level-changing collisional rate coefficient. The measurement was carried out by pumping the one-photon quadrupole-allowed $6S\rightarrow 5D_{5/2}$ transition, and monitoring the cascade $(6P_{1/2}\rightarrow 6S)/(6P_{3/2}\rightarrow 6S)$ fluorescence ratio. Since mixing can also take place between the $6P$ fine-structure levels, a second experiment was carried out in which the $6P_{3/2}$ level was pumped and the same fluorescence ratio measured. This process allowed a rather direct correction for the effects of radiation trapping and collisional mixing in the $6P$ levels. The value we obtained for the $5D$ state mixing cross-section in the present work is approximately 4 times larger than the value reported by Davanloo et al.[22] and 25 times larger than the upper limit that can be derived from the results of Wu and Huennekens.[21] We have presented some possible explanations for the discrepancies with the pulsed measurements. However, at present, we are unable to reconcile our present $5D$ fine-structure mixing cross section with the argon-ion-laser data.

ACKNOWLEDGMENTS

layed) pulsed laser to pump to high-lying Rydberg F levels that would subsequently field ionize. The high intensity of the two pulsed lasers can cause several nonlinear processes to occur, including stimulated emission on the $5D\rightarrow 6P$ transitions, various wave-mixing processes, etc. (which are not likely in the low-power cw measurements). These types of processes could rapidly depopulate the $5D$ levels in a manner that might be indistinguishable from quenching. Thus such nonlinear processes may be the cause of the larger apparent quenching rate determined in the pulsed experiment.[22]

Figure 5 shows a log-log plot of the fine-structure changing cross sections σ_{43} as a function of effective prin-

[1]A. C. Tam, T. Yabuzaki, S. M. Curry, M. Hou, and W. Happer, Phys. Rev. A 17, 1862 (1978).

[2]J. Wolnikowski, J. B. Atkinson, J. Supronowicz, and L. Krause, Phys. Rev. A 25, 2622 (1982).

[3]M. Harris and E. L. Lewis, J. Phys. B 15, L613 (1982).

[4]J. Huennekens and A. Gallagher, Phys. Rev. A 27, 1851 (1983).

[5]J. W. Parker, H. A. Schuessler, R. H. Hill, Jr., and B. G. Zollars, Phys. Rev. A 29, 617 (1984).

[6]J. Supronowicz, J. B. Atkinson, and L. Krause, Phys. Rev. A 30, 112 (1984).

[7]J. Supronowicz, J. B. Atkinson, and L Krause, Phys. Rev. A 31, 2691 (1985).

[8]L. Sirko and K. Rosiński, J. Phys. B **18**, L221 (1985).

[9]L. Sirko and K. Rosiński, J. Phys. B **19**, L279 (1986).

[10]L. Sirko and K. Rosiński, J. Phys. B **20**, L487 (1987).

[11]P. Munster and J. Marek, J. Phys. B **14**, 1009 (1981).

[12]B. G. Zollars, H. A. Schuessler, J. W. Parker, and R. H. Hill, Jr., Phys. Rev. A **28**, 1329 (1983).

[13]J. Pascale. J. M. Mestdagh, J. Cuvellier, and P. de Pujo, J. Phys. B **17**, 2627 (1984).

[14]R. Düren, E. Hasselbrink, and G. Hillrichs, Chem. Phys. Lett. **112**, 441 (1984).

[15]R. W. Berends, W. Kedzierski, and L. Krause, J. Quant. Spectrosc. Radiat. Transfer **37**, 157 (1987).

[16]J. M. Mestdagh, P. de Pujo, J. Pascale, J. Cuvellier, and J. Berlande, Phys. Rev. A **35**, 1043 (1987).

[17]L. Krause, in *The Excited State in Chemical Physics,* edited by J. W. McGowan (Wiley, New York, 1975), pp. 267–316.

[18]L. L. Vahala, P. S. Julienne, and M. D. Havey, Phys. Rev. A **34**, 1856 (1986).

[19]M. D. Havey, F. T. Delahanty, L. L. Vahala, and G. E. Copeland, Phys. Rev. A **34**, 2758 (1986).

[20]A. Ermers, T. Woschnik, and W. Behmenburg, Z. Phys. D **5**, 113 (1987).

[21]Z. Wu and J. Huennekens, J. Chem. Phys. **81**, 4433 (1984).

[22]F. Davanloo, C. B Collins, A. S. Inamdar, N. Y. Mehendale, and A. S. Naqvi, J. Chem. Phys. **82**, 4965 (1985).

[23]R. Stair, W. E. Schneider, and J. K. Jackson, Appl. Opt. **2**, 1151 (1963).

[24]T. Holstein, Phys. Rev. **72**, 1212 (1947).

[25]T. Holstein, Phys. Rev. **83**, 1159 (1951).

[26]J. Huennekens, Ph.D. thesis, University of Colorado, 1982.

[27]B. Warner, Mon. Not. R. Astron. Soc. **139**, 115 (1968).

[28]C. G. Carrington, D. N. Stacey, and J. Cooper, J. Phys. B **6**, 417 (1973).

[29]J. Huennekens and A. Gallagher, Phys. Rev. A **28**, 238 (1983).

[30]J. Huennekens, H. J. Park, T. Colbert, and S. C. McClain, Phys. Rev. A **35**, 2892 (1987).

[31]H. Bunke and R. Seiwert, *Optik u. Spektroskopie aller Wellenlängen* (Akademie Verlag, Berlin, 1962).

[32]M. Czajkowski and L. Krause, Can. J. Phys. **43**, 1259 (1965).

[33]E. Milne, J. London Math. Soc. **1**, 40 (1926).

[34]B. P. Kibble, G. Copley, and L. Krause, Phys. Rev. **153**, 9 (1967).

[35]J. S. Deech, R. Luypaert, L. R. Pendrill, and G. W. Series, J. Phys. B **10**, L137 (1977).

[36]S. Nakayama, M. Kelly, and G. W. Series, J. Phys. B **14**, 835 (1981).

[37]L. K. Lam, T. Fujimoto, A. C. Gallagher, and M. M. Hessel, J. Chem. Phys. **68**, 3553 (1978).

[38]A. N. Nesmeyanov, *Vapor Pressure of the Elements* (Academic, New York, 1963).

[39]H. Bethe and E. E. Salpeter, Handb. Phys. **35**, 88 (1957).